Covalent Organic Frameworks

DOI: 10.1002/anie.201107070

Lattice Expansion of Highly Oriented 2D Phthalocyanine Covalent Organic Framework Films**

*Eric L. Spitler, John W. Colson, Fernando J. Uribe-Romo, Arthur R. Woll, Marissa R. Giovino, Abraham Saldivar, and William R. Dichtel**

Directing the long-range order and orientation of organic semiconductors is critical to improving their performance.[1] Multicomponent films used in bulk heterojunction organic photovoltaic devices (OPVs) present the greatest difficulty, as the packing, alignment, and interfaces of two incompatible materials must be controlled in a systematic manner.[2] Strategies for manipulating molecular or polymer organization over micrometer length scales combine aspects of chemical design and processing techniques. Notable synthetic approaches include crystal engineering of acene-based organic semiconductors[3] and noncovalent assembly mediated by appended functionality,[4] including discotic liquid crystals,[5] or shape complementarity.[6] However, it remains extremely difficult to predict or design the packing of functional aromatic systems, as small chemical modifications often induce major changes in solid-state structure. Order and orientation over longer length scales are typically achieved during film formation or annealing through substrate patterning,[7] electrical or magnetic field alignment,[8] zone refining,[9] or diblock copolymer phase separation.[10]

Covalent organic frameworks (COFs) are an emerging class of materials that organize and align organic semiconductors predictably.[11–14] COF syntheses use reversible covalent bond-forming reactions to link molecular building blocks into periodic two-dimensional (2D) or three-dimensional networks. The 2D variants crystallize into layered structures containing stacked aromatic subunits ideal for interlayer exciton and charge transport.[15–17] 2D COFs exhibit several desirable and unique features: The length and relative orientation of their linking groups determine the lattice structure, in contrast to the unpredictable packing of traditional organic semiconductors. Also, their permanent porosity provides a continuous, high surface area interface for additional functionalization. COFs are typically isolated as insoluble and unprocessable powders not easily incorporated into devices, but we recently synthesized oriented COF thin films on single-layer graphene (SLG).[18] These films would be well suited for ordered heterojunctions except their pores are too small to accommodate continuous domains of complementary semiconductors. Feasible lattice expansion is a tenet of reticular chemistry but is largely undemonstrated in COFs. Only the smallest possible pore width (2.3 nm) of the square phthalocyanine network most relevant for OPVs has been reported.[13] Here we describe 2D Zn phthalocyanine (ZnPc) COFs with expanded diagonal pore widths of 2.7, 3.4, 4.0, and 4.4 nm (Figure 1), by using the longest linkers incorporated into COFs thus far. We prepared each COF under similar reaction conditions, both as an insoluble powder and as an oriented film on SLG. One of the ZnPc COF films exhibits superior crystallinity and vertical alignment compared to any other film we have prepared. Tuning the porosity and composition of these materials while maintaining their desirable topology demonstrates the versatility and power of the COF approach.

The COFs were synthesized as powders by condensing Zn octahydroxyphthalocyanine (**5**) with each of the four different linear diboronic acid linkers shown in Scheme 1. The COF syntheses were performed in sealed glass ampoules in 2:1, 3:1, or 5:1 mixtures of dioxane:MeOH at 120 °C for 72 h. The COFs were reproducibly isolated as insoluble microcrystalline powders whose FT-IR spectra confirmed the formation of boronate ester linkages resonant near 1340 cm^{-1} and showed attenuated hydroxy stretches (see Supporting Information, Figures S8–S17). The COFs display excellent thermal stability, each retaining about 90% of its mass upon heating to 350 °C (Figure S26). **ZnPc-Py COF** and **ZnPc-NDI COF** crystallize as needle-like structures, while **ZnPc-DPB COF** forms rough irregular sheets and **ZnPc-PPE COF** forms smooth μm-size aggregated spheroids, as observed by scanning electron microscopy (SEM, Figure S31).

The crystallinity of the synthesized COFs was determined by powder X-ray diffraction (PXRD). As observed in Figure 2, each of the COFs displays a PXRD pattern with a large diffraction peak at 2θ ($Cu_{K\alpha}$ radiation) and d spacings of 3.20° (27.6 Å) for **ZnPc-Py COF**, 2.67° (33.1 Å) for **ZnPc-DPB COF**, 2.44° (36.2 Å) for **ZnPc-NDI COF**, and 2.36°

[*] Dr. E. L. Spitler, J. W. Colson, Dr. F. J. Uribe-Romo, M. R. Giovino, A. Saldivar, Prof. Dr. W. R. Dichtel
Department of Chemistry and Chemical Biology
Cornell University, Baker Laboratory
Ithaca, NY 14853 (USA)
E-mail: wdichtel@cornell.edu
Dr. A. R. Woll
Cornell High Energy Synchrotron Source (CHESS)
Ithaca, NY 14853 (USA)

[**] This research was supported by the NSF CAREER award (CHE-1056657), and a 3M Nontenured Faculty Award. This work is also based upon research conducted at the Cornell High Energy Synchrotron Source (CHESS), which is supported by the NSF and the NIH/National Institute of General Medical Sciences under NSF award DMR-0936384. We also made use of the Cornell Center for Materials Research facilities with support from the NSF Materials Research Science and Engineering Centers (MRSEC) program (DMR-0520404). J.W.C. acknowledges the award of a Graduate Research Fellowship from the NSF. E.L.S. acknowledges the award of the American Competitiveness in Chemistry postdoctoral fellowship (ACC-F) from the NSF (CHE-0936988).

Supporting information for this article is available on the WWW under http://dx.doi.org/10.1002/anie.201107070.

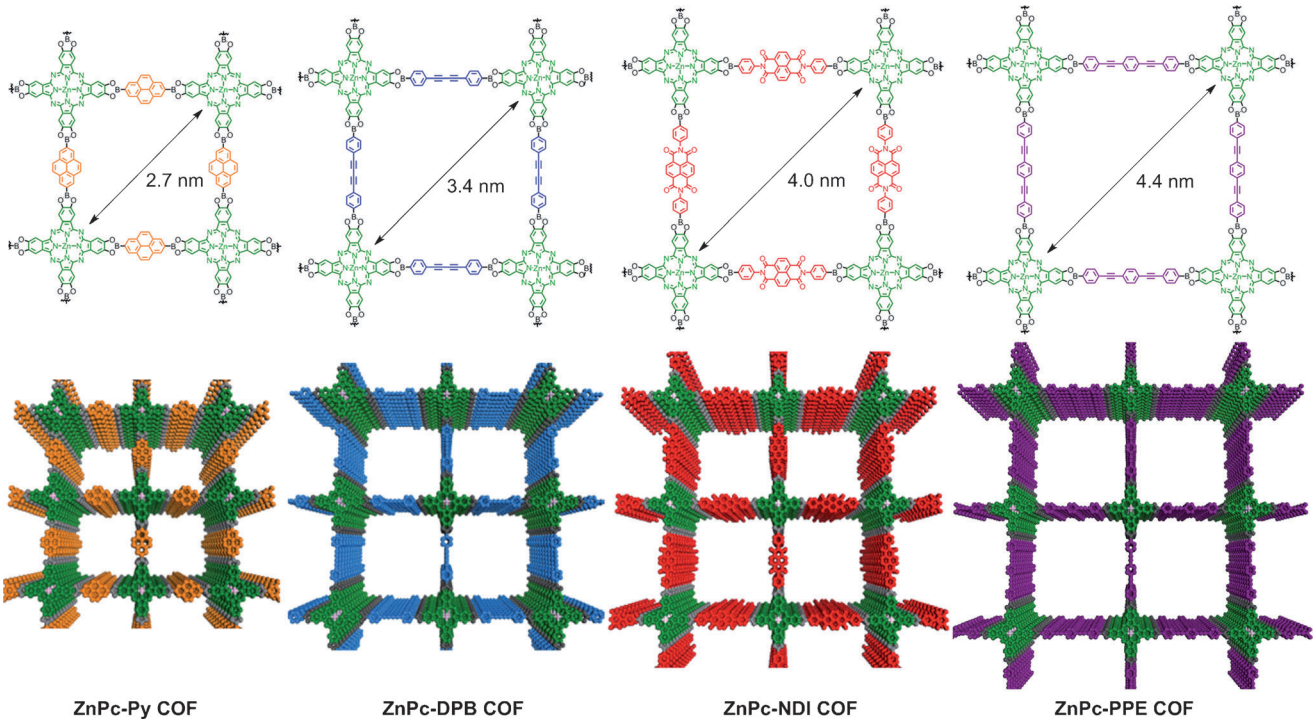

Figure 1. Chemical and extended structures of the expanded ZnPc COFs. Each COF forms a two-dimensional layered network containing zinc phthalocyanines joined by (left to right) pyrene, diphenylbutadiyne, naphthalenediimide, and phenylbis(phenylethynyl) units.

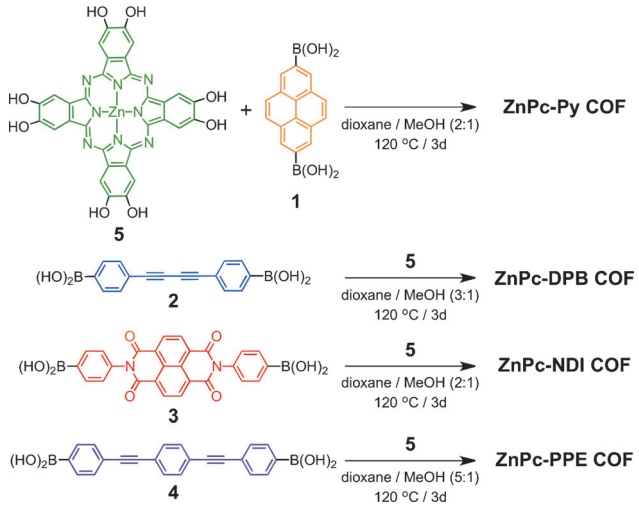

Scheme 1. Synthesis of 2D ZnPc covalent organic frameworks.

(37.4 Å) for **ZnPc-PPE COF**. Additionally, all the COFs show a small broad peak at 26.58° (ca. 3.35 Å), which is similar to those observed in other 2D COFs and other 2D layered materials, such as graphite and boron nitride.[19] The diffraction peaks of each COF are consistent with a primitive tetragonal unit cell in which the (100), (200), (300), (400), (500) and (001) reflections were observed, as well as the weak (110) reflection for the **ZnPc-DPB** and **ZnPc-PPE COFs**. Each COF is comprised of square-shaped ZnPc building blocks and linear linkers of varying length that form square planar sheets that stack in a highly symmetric eclipsed or nearly eclipsed fashion. Based on this hypothesis, we modeled the eclipsed crystal structures of each material and simulated their powder X-ray diffraction patterns using the Materials Studio suite of programs. The COFs display diffraction patterns consistent with the simulations, crystallizing as cofacially stacked two-dimensional sheets with *P*4/*mmm* symmetry, similar to the free base and Ni phthalocyanine COFs linked by phenylene-bis(boronic acid).[13,14,16] We also considered a staggered structure (*I*4/*mmm*) in which the ZnPc moieties in adjacent layers are offset by half a unit cell distance along the *a* and *b* axes (Figure S25). The simulated PXRD patterns of these structures do not match the experiments. The excellent agreement between simulated and observed patterns facilitated indexing of the observed peaks following Pawley refinement (Figures S21–S24).[13,16] The refined patterns resulted in unit cell parameters of $a = 26.980$ Å and $c = 3.338$ Å for **ZnPc-Py COF**; $a = 32.183$ Å and $c = 3.356$ Å for **ZnPc-DPB COF**; $a = 35.701$ Å and $c = 3.361$ Å for **ZnPc-NDI COF**; and $a = 38.533$ Å and $c = 3.367$ Å for **ZnPc-PPE COF**. Despite the good crystallinity of these samples, the X-ray diffraction data do not preclude small deviations from perfectly eclipsed stacking. Based on typical π–π stacking geometries and DFT calculations performed on other boronate-linked 2D COFs,[20] it is likely that adjacent layers are offset by around 1.7 Å. These calculations should be considered in future models of interlayer exciton and charge transport.[17] Diffuse reflectance absorbance spectroscopy of the COF powders (Figure S18) shows that each COF absorbs light throughout the visible and near-IR regions. The highly absorbent ZnPc chromophore dominates the spectrum of each material, and the spectra of the four COFs are very similar. They are red-shifted relative

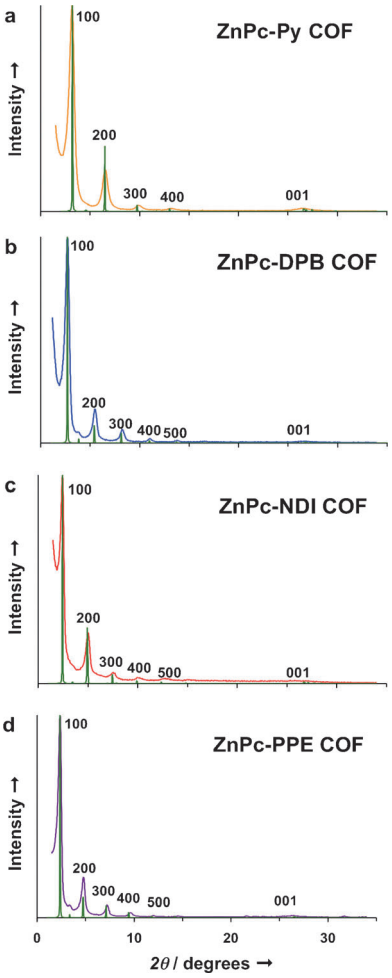

Figure 2. Experimental vs. predicted (green) PXRD patterns of a) **ZnPc-Py COF**, b) **ZnPc-DPB COF**, c) **ZnPc-NDI COF**, and d) **ZnPc-PPE COF**.

to H_2Pc COFs and very similar to the phenylene-linked NiPc COF, which was photoconductive under NIR excitation.[16]

The porosity and surface areas of the ZnPc COFs were characterized by N_2 adsorption after activating the powders by washing with toluene and heating under vacuum. The COFs exhibit Type IV isotherms typical of mesoporous materials (Figure 3), with initial adsorption into the pores at low relative pressures ($0.01 < P/P_0 < 0.10$).[21] Desorption follows the same general pathway, indicating reversible N_2 uptake. The Brunauer–Emmett–Teller (BET) surface-area model was applied to the $0.02 < P/P_0 < 0.25$ region of the curves (Figures S27–S30), which provided BET surface areas of 420 $m^2 g^{-1}$ for **ZnPc-Py COF**, 485 $m^2 g^{-1}$ for **ZnPc-DPB COF**, 490 $m^2 g^{-1}$ for **ZnPc-NDI COF**, and 440 $m^2 g^{-1}$ for **ZnPc-PPE COF**. These surface areas are similar to previous H_2Pc and NiPc COFs.[13,14,16] Application of non-local density functional theory (NLDFT) models over the measured isotherms yielded pore-size distribution plots, from which average pore sizes were obtained (Figures S33–S36). The average pore sizes determined were 31 Å, for **ZnPc-Py COF**, **ZnPc-DPB COF**, and **ZnPc-NDI COF**, and 34 Å for **ZnPc-PPE COF**, which correlate in reasonable agreement with the predicted numbers from the modeled crystal structures.

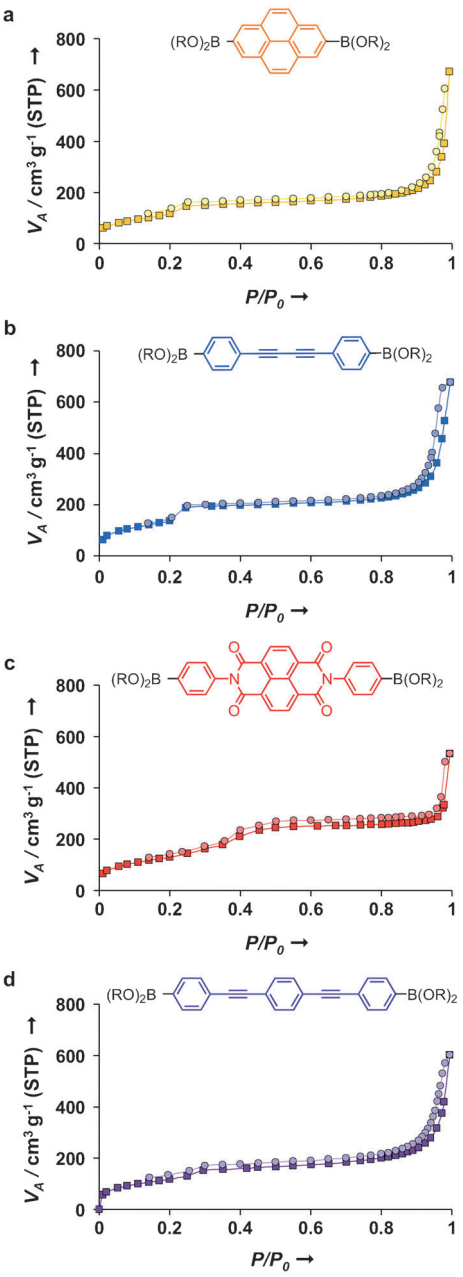

Figure 3. N_2 uptake and surface area analysis of the ZnPc COFs. Adsorption (squares) and desorption (circles) isotherms for a) **ZnPc-Py COF** (gold), b) **ZnPc-DPB COF** (blue), c) **ZnPc-NDI COF** (red), and d) **ZnPc-PPE COF** (purple).

Despite their intriguing structures, COF powders are difficult to interface to electrodes or incorporate into devices. Thus, we grew each 2D ZnPc COF as a crystalline, vertically oriented thin film on a transparent SLG-functionalized fused silica substrate (SLG/SiO_2). For example, **ZnPc-Py COF** thin films were obtained by condensing **1** and **5** in a mixture of dioxane, MeOH, *N*,*N*-dimethylacetamide (DMA), and 1,2-dichlorobenzene (DCB) (3:1:2:1 v/v) in the presence of SLG/SiO_2. This solvent combination provided each of the ZnPc COFs as crystalline, oriented films and was modified from the DMA/DCB mixture employed by Jiang et al.[16] for a NiPc

COF powder. Interestingly, a DMA/DCB mixture lacking the other cosolvents provided crystalline COF films on the SLG whose grains showed no preferred orientation. The films were characterized using grazing incidence X-ray diffraction (GID, Figure 4a) to assess their crystallinity and preferred orientation. The GID pattern of the **ZnPc-Py COF** film shows scattering intensity at 0.22 $Å^{-1}$, 0.46 $Å^{-1}$, 0.69 $Å^{-1}$, 0.92 $Å^{-1}$, corresponding to the (100), (200), (300), and (400) peaks observed in the powder samples. This intensity is concentrated near $Q_\perp = 0$ $Å^{-1}$, indicating that the *c*-axis of the COF is oriented normal to the substrate surface. The (001) Bragg peak that appears at $Q_\parallel = 1.83$ $Å^{-1}$ in powder samples, absent in the GID experiment, further confirms that the *c*-axis is oriented normal to the substrate. Instead, this peak is observed as a diffuse arc of scattering from $Q_\perp = 1.85$ to 1.90 $Å^{-1}$ in measurements performed at large out-of-plane diffraction angles (see Figure 5d), indicating an angular spread of the stacking direction, or mosaicity, of ±11°. Cross-sectional SEM obtained by milling the sample with a Ga^+ focused ion beam indicates a (400 ± 12) nm thick continuous film.

Similar crystalline, vertically oriented **ZnPc-NDI** and **ZnPc-PPE COF** thin films were obtained by condensing diboronic acid linkers **3** or **4** with **5** under similar conditions. GID patterns of these films are similar to that of **ZnPc-Py COF**, albeit with scattering intensity at smaller values of $Q_\parallel$, corresponding to larger lattices. The (001) Bragg peak that appears at $Q_\parallel = 1.83$ $Å^{-1}$ in each powder sample is again absent in the GID of each film but is found to be similar to that shown in Figure 5d in out-of-plane scans. Cross-sectional SEM indicate (580 ± 84) nm and (200 ± 18) nm thick films for the **ZnPc-NDI** (Figure 4d) and **ZnPc-PPE COF** (Figure 4f), respectively.

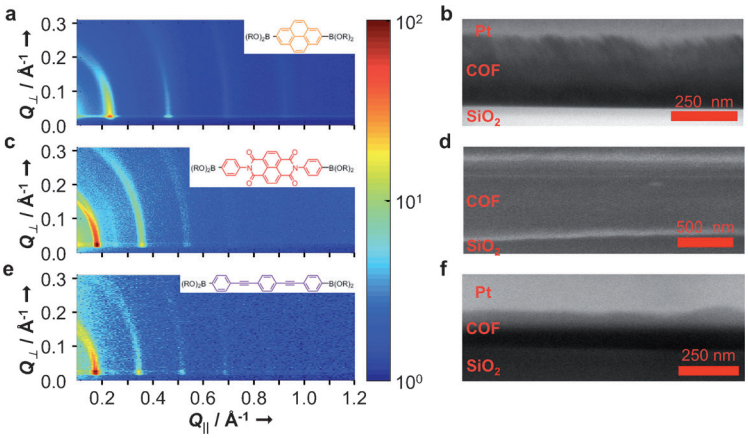

Figure 4. Grazing incidence X-ray diffraction patterns and cross-sectional SEM for a,b) **ZnPc-Py COF**, c,d) **ZnPc-NDI COF**, and e,f) **ZnPc-PPE COF**. The maximum intensity of each (100) Bragg peak is normalized to 100 counts.

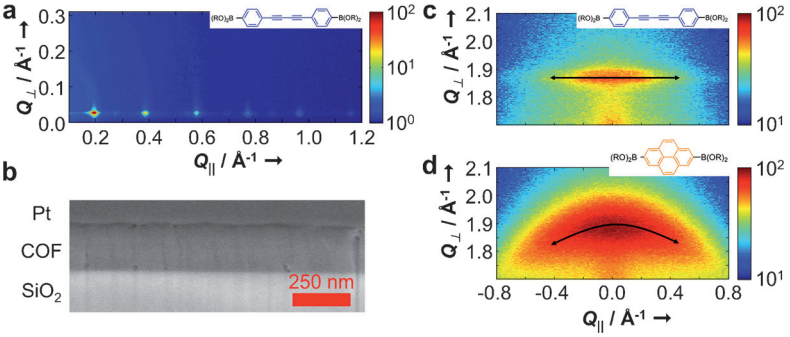

Figure 5. Superior crystallinity and alignment of a **ZnPc-DPB COF** film. a) Grazing incidence X-ray diffraction pattern and b) cross-sectional SEM of **ZnPc-DPB COF**. The intensity of the off-specular projection of the (001) Bragg peak for **ZnPc-DPB COF** (c) is flat with respect to $Q_\perp$, indicating nearly zero mosaicity, while that of the **ZnPc-Py COF** (d) is representative of other COF films and shows an arc of scattering typical of less ideal vertical alignment.

Although grown under the same conditions, the **ZnPc-DPB COF** films show superior crystallinity and vertical alignment. The GID (Figure 5a) of a (294 ± 6) nm thick film (Figure 5b) indicates near complete localization of the scattering intensity near $Q_\perp = 0$ $Å^{-1}$. In contrast to Figures 4a,c,e, the peak intensity at $Q_\perp = 0.028$ $Å^{-1}$ is over 20 times higher than that in the diffuse arc of scattering extending towards larger $Q_\perp$, suggesting a mosaic spread below 0.2°. Peaks at 0.19 $Å^{-1}$, 0.28 $Å^{-1}$, 0.39 $Å^{-1}$, 0.58 $Å^{-1}$, and 0.78 $Å^{-1}$ correspond to the (100), (110), (200), (300), and (400) peaks observed in the powders. (500) and (600) Bragg peaks not observed in the PXRD pattern (Figure 3b) are observed at 0.97 $Å^{-1}$ and 1.16 $Å^{-1}$, respectively, in the GID experiment. The off-specular (001) Bragg peak at $Q_\parallel = 1.86$ $Å^{-1}$ (Figure 5c) is distinct from **ZnPc-Py COF** (Figure 5d) or other 2D ZnPc COFs. First, the intensity distribution is flat, rather than curved, indicating that its width in $Q_\parallel$ arises from finite lateral grain size, rather than mosaic spread. This observation is consistent with the low mosaic spread deduced from Figure 5a. Second, the background-subtracted width of the peak along $Q_\perp$ is narrower than that in **ZnPc-Py COF** (Figure 5d), indicating a longer correlation length along the stacking direction. This peak width is resolution-limited due to the geometric expansion of the beam as a consequence of the grazing incidence geometry. Additional scans (Figures S37, S38) performed with improved resolution indicate a correlation length in the stacking direction of around 31 nm (ca. 94 layers), far exceeding that found in other COF films. For example, the **ZnPc-Py COF** data in Figure 5d, which is not resolution-limited, gives a correlation length of ca. 4 nm or 12 layers. We attribute the **ZnPc-DPB COF**'s superior order partially to its diphenylbutadiyne linker, which can readily adopt a coplanar conformation needed during COF formation, although it may prove possible to obtain similar order in the other ZnPc COF films through further optimization.

COF films offer an unprecedented opportunity to organize and orient functional π-electron systems into robust periodic structures predictably through chemical synthesis.

We have progressively expanded the pore size of the ZnPc lattice well into the mesoporous regime, such that many complementary materials, including fullerene acceptors, might form continuous nanostructured domains alongside the vertically stacked ZnPc macrocycles. The superior crystallinity and nearly zero mosaic spread of the diphenyl butadiyne-linked materials is particularly promising for forming nearly perfect ordered heterojunction structures.

Received: October 6, 2011
Revised: November 22, 2011
Published online: January 3, 2012

Keywords: covalent organic frameworks · mesoporous materials · organic electronics · supramolecular chemistry · thin films

[1] a) H. N. Tsao, K. Müllen, *Chem. Soc. Rev.* **2010**, *39*, 2372; b) M. Mas-Torrent, C. Rovira, *Chem. Rev.* **2011**, *111*, 4833.
[2] a) X. Yang, J. Loos, *Macromolecules* **2007**, *40*, 1353; b) B. C. Thompson, J. M. J. Fréchet, *Angew. Chem.* **2008**, *120*, 62; *Angew. Chem. Int. Ed.* **2008**, *47*, 58; c) M. D. Perez, C. Borek, S. R. Forrest, M. E. Thompson, *J. Am. Chem. Soc.* **2009**, *131*, 9281; d) C. Groves, O. G. Reid, D. S. Ginger, *Acc. Chem. Res.* **2010**, *43*, 612.
[3] a) J. E. Anthony, *Chem. Rev.* **2006**, *106*, 5028; b) A. L. Briseno, S. C. B. Mannsfeld, X. Lu, Y. Xiong, S. A. Jenekhe, Z. Bao, Y. Xia, *Nano Lett.* **2007**, *7*, 668.
[4] a) L. Schmidt-Mende, A. Fechtenkötter, K. Müllen, E. Moons, R. H. Friend, J. D. MacKenzie, *Science* **2001**, *293*, 1119; b) V. Percec, M. Glodde, T. K. Bera, Y. Miura, I. Shiyanovskaya, K. D. Singer, V. S. K. Balagurusamy, P. A. Heiney, I. Schnell, A. Rapp, H. W. Spiess, S. D. Hudson, H. Duan, *Nature* **2002**, *417*, 384; c) N. Kumaran, P. A. Veneman, B. A. Minch, A. Mudalige, J. E. Pemberton, D. F. O'Brien, N. R. Armstrong, *Chem. Mater.* **2010**, *22*, 2491; d) R. Berger, G. Resnati, P. Metrangolo, E. Weber, J. Hulliger, *Chem. Soc. Rev.* **2011**, *40*, 3496.
[5] a) S. Kumar, *Chem. Soc. Rev.* **2006**, *35*, 83; b) S. Sergeyev, W. Pisula, Y. H. Geerts, *Chem. Soc. Rev.* **2007**, *36*, 1902.
[6] A. A. Gorodetsky, C.-Y. Chiu, T. Schiros, M. Palma, M. Cox, Z. Jia, W. Sattler, I. Kymissis, M. Steigerwald, C. Nuckolls, *Angew. Chem.* **2010**, *122*, 8081; *Angew. Chem. Int. Ed.* **2010**, *49*, 7909.
[7] a) E. W. Edwards, M. F. Montague, H. H. Solak, C. J. Hawker, P. F. Nealey, *Adv. Mater.* **2004**, *16*, 1315; b) B. D. Gates, Q. Xu, M. Stewart, D. Ryan, C. G. Willson, G. M. Whitesides, *Chem. Rev.* **2005**, *105*, 1171; c) J. Hoogboom, P. M. L. Garcia, M. B. J. Otten, J. A. A. W. Elemans, J. Sly, S. V. Lazarenko, T. Rasing, A. E. Rowan, R. J. M. Nolte, *J. Am. Chem. Soc.* **2005**, *127*, 11047.
[8] a) M. L. Bushey, T.-Q. Nguyen, C. Nuckolls, *J. Am. Chem. Soc.* **2003**, *125*, 8264; b) I. O. Shklyarevskiy, P. Jonkheijm, N. Stutzmann, D. Wasserberg, H. J. Wondergem, P. C. M. Christianen, A. P. H. J. Schenning, D. M. de Leeuw, Z. Tomovic, J. Wu, K. Müllen, J. C. Maan, *J. Am. Chem. Soc.* **2005**, *127*, 16233; c) H. Monobe, K. Awazu, Y. Shimizu, *Adv. Mater.* **2006**, *18*, 607.
[9] A. Tracz, J. K. Jeszka, M. D. Watson, W. Pisula, K. Müllen, T. Pakula, *J. Am. Chem. Soc.* **2003**, *125*, 1682.
[10] a) R. A. Segalman, B. McCulloch, S. Kirmayer, J. J. Urban, *Macromolecules* **2009**, *42*, 9205; b) V. Ho, B. W. Boudouris, B. L. McCulloch, C. G. Shuttle, M. Burkhardt, M. L. Chabinyc, R. A. Segalman, *J. Am. Chem. Soc.* **2011**, *133*, 9270.
[11] a) A. P. Côté, A. I. Benin, N. W. Ockwig, M. O'Keeffe, A. J. Matzger, O. M. Yaghi, *Science* **2005**, *310*, 1166; b) A. P. Côté, H. M. El-Kaderi, H. Furukawa, J. R. Hunt, O. M. Yaghi, *J. Am. Chem. Soc.* **2007**, *129*, 12914; c) S. Wan, J. Guo, J. Kim, H. Ihee, D. L. Jiang, *Angew. Chem.* **2008**, *120*, 8958; *Angew. Chem. Int. Ed.* **2008**, *47*, 8826; d) X. Feng, L. Chen, Y. Dong, D. Jiang, *Chem. Commun.* **2011**, *47*, 1979.
[12] a) R. W. Tilford, W. R. Gemmill, H. C. zur Loye, J. J. Lavigne, *Chem. Mater.* **2006**, *18*, 5296; b) R. W. Tilford, S. J. Mugavero, P. J. Pellechia, J. J. Lavigne, *Adv. Mater.* **2008**, *20*, 2741.
[13] E. L. Spitler, W. R. Dichtel, *Nat. Chem.* **2010**, *2*, 672.
[14] E. L. Spitler, M. R. Giovino, S. L. White, W. R. Dichtel, *Chem. Sci.* **2011**, *2*, 1588.
[15] S. Wan, J. Guo, J. Kim, H. Ihee, D. L. Jiang, *Angew. Chem.* **2009**, *121*, 5547; *Angew. Chem. Int. Ed.* **2009**, *48*, 5439.
[16] X. Ding, J. Guo, X. Feng, Y. Honsho, J. Guo, S. Seki, P. Maitarad, A. Saeki, S. Nagase, D. Jiang, *Angew. Chem.* **2011**, *123*, 1325; *Angew. Chem. Int. Ed.* **2011**, *50*, 1289.
[17] S. Patwardhan, A. A. Kocherzhenko, F. C. Grozema, L. D. A. Siebbeles, *J. Phys. Chem. C* **2011**, *115*, 11768.
[18] J. W. Colson, A. R. Woll, A. Mukherjee, M. P. Levendorf, E. L. Spitler, V. B. Shields, M. G. Spencer, J. Park, W. R. Dichtel, *Science* **2011**, *332*, 228.
[19] E. K. Sichel, R. E. Miller, M. S. Abrahams, C. J. Buiocchi, *Phys. Rev. B* **1976**, *13*, 4607.
[20] a) W. Zhou, H. Wu, T. Yildirim, *Chem. Phys. Lett.* **2010**, *499*, 103; b) B. Lukose, A. Kuc, T. Heine, *Chem. Eur. J.* **2011**, *17*, 2388; c) E. L. Spitler, B. T. Koo, J. L. Novotney, J. W. Colson, F. J. Uribe-Romo, G. D. Gutierrez, P. Clancy, W. R. Dichtel, *J. Am. Chem. Soc.* **2011**, DOI: 10.1021/ja206242v.
[21] K. S. W. Sing, D. H. Everett, R. A. W. Haul, L. Moscou, R. A. Pierotti, J. Rouquerol, T. Siemieniewska, *Pure Appl. Chem.* **1985**, *57*, 603.

